Epsilon-near-zero metalenses operating in the visible

V. Pacheco-Peña,[1,a)] M. Navarro-Cía,[2,3,b)] and M. Beruete,[1,4c)]

[1]Antennas Group-TERALAB, Universidad Pública de Navarra, Campus Arrosadía, 31006 Pamplona, Spain

[2]Optical and Semiconductor Devices Group, Department of Electrical and Electronic Engineering, Imperial College London, London SW7 2BT, UK

[3]School of Physics and Astronomy, University of Birmingham, Birmingham B15 2TT, UK

[4] Institute of Smart Cities, Public University of Navarra, 31006, Pamplona, Spain

Several converging lenses working in the permittivity near to zero (ENZ) regime at optical frequencies are designed using an array of metal-dielectric-metal plasmonic waveguides. These plasmonic waveguides show a dispersive nature that enable to mimic an effective ENZ medium when using the fast wave transverse electric (TE_1) mode near its cut-off wavelength. By arranging multiple plasmonic waveguides with the correct engineered dimensions, several metalenses, including graded index (GRIN) ones, and diffractive optical elements (i.e., zoned metalenses) are proposed. The metalenses are designed at λ_0 = 474.9nm (f = 631.67THz) with a focal length of 10.75λ_0. Numerical results demonstrate that the best performance is obtained for the case of the GRIN metalens in terms of the focal position, transversal resolution and thickness, reducing its volume up to ~52.3% with respect to the smooth-profiled plano-concave metalens.

Keywords: ENZ, optical focusing, focusing, metamaterials, lenses

[a)] Electronic mail: victor.pacheco@unavarra.es

[b)] Electronic mail: M.Navarro-Cia@bham.ac.uk

[c)] Electronic mail: miguel.beruete@unavarra.es

1. Introduction

Fascinated by the unprecedented control of the electromagnetic waves offered by metamaterials, the scientific community has devoted a great deal of effort to tailor their intrinsic properties.[1,2] By correctly engineering the dimensions, geometry and materials composing of the metamaterial's unit, different electromagnetic responses can be synthesized, including values of the effective permittivity (ε) and permeability (μ) not available in nature.[3]

Within the world of metamaterials, those with permittivity approaching to zero, usually called ε-near-zero (ENZ), are very attractive due to their promising features such as an almost infinite effective wavelength and a close to zero group velocity of the waves traveling through them. These properties give rise to exciting phenomena such as squeezing, supercoupling and tunneling, which were first reported and experimentally demonstrated at microwave frequencies, where metals can be treated as perfect electric conductors.[4–7] By using adequate metal models, the concept of ENZ metamaterials has been scaled down to near infrared and visible wavelengths.[8–10] The field has matured significantly over the last years and several applications of ENZ-media have been proposed such as dielectric sensing,[11] nanocircuits,[12] Fourier transformation[13] and beamshaping. [14–18]

In this work, the dispersion of metal-dielectric-metal plasmonic waveguides is exploited to artificially mimic an ENZ medium at optical wavelengths by working near the cut-off of the transverse electric TE_1 mode. This mode is intrinsically dispersive and can be modeled with a Drude function.[19] Hence, by working near its cut-off region (which depends on the geometrical dimensions of the plasmonic waveguide), it is possible to emulate the performance of an ENZ medium. The dispersion of such waveguide is then studied when the percentage of dielectric and metal per unit cell is changed, demonstrating that the ENZ performance may be emulated within the whole visible spectrum by simply adjusting this parameter. Built upon such ENZ media, several types of focusing metalenses are studied at λ_0 = 474.9 nm (f = 631.67 THz). Namely, a plano-concave smooth-profiled metalens and its step-wise approximation, a zoned metalens and a graded index (GRIN) metalens. The focusing performance of these four metalenses is then evaluated in terms of the focal length (FL), depth of focus (DF) and full-width at half-maximum (FWHM) demonstrating that the best performance is obtained for the GRIN metalens. This metalens has the additional benefit that offers a reduction of volume ~52% compared with the full concave profiled metalens.

2. Metal-Dielectric-Metal waveguide

To begin with, let us analyze the features of the plasmonic metal-dielectric-metal parallel plate waveguide that will be used throughout this work. The waveguide is shown in Figure 1(a) and has an arbitrary length of l_z = 1000nm and thickness d_x = 200nm. It consists of a dielectric slab (Silicon dioxide SiO_2) of thickness h_x sandwiched in between two plates of silver (Ag) with a complex permittivity fitting the Palik's experimental data.[20] The waveguide is infinite along y.

As it is well known, a plasmonic parallel plate waveguide can support two types of modes:[21] surface plasmon modes (SPP) where the propagation constant is larger than the wavenumber in free-space ($\beta > k_o$) [also known as slow wave modes since they fall beyond the cone of light] and the parallel plates waveguide modes with the complementary performance ($\beta < k_o$) [also named as fast wave modes]. We are interested in the second group of modes since it is not possible to use the SPP modes to artificially create an ENZ medium; SPP modes require a negative permittivity in order to exist. Thus, we look at the fundamental mode for the parallel plate plasmonic waveguide with the electric field parallel to the plates (E_y); i.e., the TE_1 mode. It is important to note that, since the electric field is not perpendicular but parallel to the metal plates of the plasmonic waveguide, the TM mode is not excited. Hence, there is not a background mode interfering with the desired mode as it could happen if the orthogonal polarization (E_x) would be used. For the orthogonal polarization (E_x), the wise approach to emulate an ENZ medium is to work at the cut-off of the fundamental rectangular plasmonic waveguide TE_{01} mode. [23,24]

In our case, TE_1 mode is a fast wave mode whose dispersion relation, assuming semi-infinite metals, can be expressed as follows[22]:

$$\tan\left(\frac{h_x}{2}\sqrt{\varepsilon_{SiO_2}k_0^2-\beta^2}\right)=\frac{\sqrt{\beta^2-\varepsilon_{Ag}k_0^2}}{\sqrt{\varepsilon_{SiO_2}k_0^2-\beta^2}} \qquad (1)$$

where ε_{SiO2} is the permittivity of the silicon dioxide in the middle of the waveguide, ε_{Ag} is the complex permittivity of the metal (silver in our case), k_0 is the wave number in free space and β is the propagation constant of the TE mode. From (1) one can conclude that the dispersion of the plasmonic waveguides is directly related to the thickness of the dielectric slab sandwiched between metallic plates. To look at this closer, the real part of β using (1) normalized with respect to the wavenumber in vacuum (i.e., Re(β) / k_0) as a function of the free-space wavelength (λ_0) and transversal dimension (h_x)

is shown in Figure 1(b). Three regions of operation are observed: a) the cut-off region where the mode does not propagate in the structure, b) the propagation region where the mode exists and propagates in the waveguide and finally c) the ENZ region. Within the ENZ region, $\mathrm{Re}(\beta)/k_0 << 1$, i.e., it is possible to emulate an ENZ artificial medium working at these wavelengths.

The previous analytical calculation is a good starting point to ground the physics. However, it is only valid for the case of a single parallel plate plasmonic waveguide. For the application in this manuscript, however, where several parallel plate plasmonic waveguides with thin metal walls are arranged next to each other, the potential coupling between neighbors should be considered. To this end, we use as an unit cell the waveguide shown in Figure 1(a) and employ the frequency domain solver of the commercial software CST Microwave Studio™ to retrieved from the S-parameters the effective permittivity of the arrayed configuration.[25] Periodic boundary conditions were imposed on the left, right, top and bottom sides of the waveguide in order to realize an infinite array of waveguides along both *x*- and *y*- axes. The effective permittivity was retrieved for two different metal filling fractions: a 10% and 48% metal thickness which correspond to a thickness of the dielectric of h_x = 180 nm and h_x = 104 nm, respectively, see Figure 1(c) and 1(d), respectively. For the 10% case, the ENZ region emerges at 868.3 nm, where the complex permittivity is 0.0034+ *i*0.0845. For the 48% case, the complex permittivity is 0.0951+ *i*0.1804 at 474.9nm. This confirms the ability to tune the ENZ performance over a wide spectral range using the plasmonic parallel plate waveguide. For the sake of completeness, Figure 1(e) shows the retrieved effective complex permittivity for the case of the plasmonic waveguide shown in Figure 1(d) but with an increased length (l_z = 2600nm). For such length, Fabry-Perot resonances appear in the spectrum of interest, resulting into a distortion of the ideal Drude response. This effect is not observed for the case shown in Figure 1(c-d) due to the reduced length of these plasmonic waveguides.

Let us now evaluate the field distribution for the case of the waveguide with dielectric thickness h_x = 104nm and length l_z = 1000nm [see Figure 1(d)]. For this study, the same solver was used as previously and the plasmonic waveguides were illuminated with a vertically polarized (E_y) plane-wave. An electric probe was placed at the output of the waveguide to record the transmitted electric field. The numerical results of the normalized E_y-field as a function of wavelength is shown in Figure 2(a) where two peaks of transmission emerge: one related to the ENZ regime and the second to the Fabry-Perot resonance.

To support the latter statement, the numerical results of the phase distribution of the E_y-field along the optical *z*-axis together with the normalized field distribution on the *yz*-plane are shown in Figure 2(b, c) for the first and second transmission peaks, respectively. The phase distribution inside the waveguide is almost constant at λ_0 = 474.9nm [Figure 2(b)] while it is not the case for λ_0 = 445.2nm [Figure 2(c)]. This corroborates the assumption that each peak corresponds to the ENZ regime and the Fabry-Perot resonance, respectively.[16] The normalized propagation constant extracted from the phase difference between the output and the input of the waveguide is 0.27 and 0.7 at λ_0 = 474.9nm and λ_0 = 445.2nm, respectively, which represent an effective permittivity of ε_{eff} = 0.09 and ε_{eff} = 0.38. By working at λ_0 = 474.9nm, the plasmonic waveguide actually emulates an ENZ medium with almost zero values of phase variation and propagation constant.

3. Design and Results

Using as a reference building block the parallel plate plasmonic waveguide studied in detail before with a dielectric thickness of h_x = 104nm and length l_z = 1000nm, we design here several ENZ focusing metalenses with focal length of $FL = 10.75\lambda_0$: a plano-concave smooth-profiled metalens, its step-wise approximation, and a zoned metalens and a graded index (GRIN) metalens. For simplicity, all our focusing elements have an input flat interface.

3.1. Plano-concave smooth-profiled and step-wise metalenses

To begin with, let us first analyze the focusing properties of the simplest metalens with the input face flat. As it is known, in order to produce optical focusing, the output face of a lens should be designed with a convex or concave profile depending on whether the refractive index of the lens is larger than 1 (such as in natural dielectrics) or smaller than 1 (our case).[26] Based on this, the designed full plano-concave metalens working at the previous described wavelength and FL is shown in Figure 3(a). Note that this metalens has a smooth output surface in order to follow the corresponding circular profile. Also, a step-wise metalens is designed following the same profile, as shown in Figure 3(d).

With the aim of evaluating the focusing performance of both metalenses under a vertically (E_y) polarized plane-wave illumination, the transient solver of the commercial software CST Microwave Studio™ was used. Electric planes were defined at the top and bottom of the structures to make them infinite along the *y*-axis, i.e., cylindrical metalenses, whereas open boundary conditions were applied to the rest of the boundaries to emulate an isolated metalens in free-space.

The numerical results of the power distribution on the focal plane (*xz*-plane) for the plano-concave smooth and step-wise profiles are shown in Figure 3(b, e), respectively, at the designed wavelength of λ_0 = 474.9 nm. It can be observed that both metalenses produce a focus at the output plane with a FL of $14.4\lambda_0$ and $14.23\lambda_0$, respectively. Note that the FL is similar for both cases but they are strongly deviated $3.65\lambda_0$ and $3.48\lambda_0$, respectively, from the designed value ($10.75\lambda_0$). This is mainly due to the influence of the waveguides far away from the central ones. Each waveguide in the array shows a slightly different dispersion due to their notable length difference, as it has been shown in Figure 1(e) for the case of an increased length of a plasmonic waveguide. The Fabry-Perot resonances that appear in longer waveguides deteriorate the ideal Drude response of the plasmonic waveguides, destroying the homogeneity of the lens in terms of effective permittivity. As a consequence, the different parts of the metalens do not work together coherently to produce the desirable focusing. This problem will be solved in the following sections using the zoning and the GRIN techniques, whereby the length of the plasmonic waveguides are kept close. To evaluate the focusing performance quantitatively, the normalized power distribution along the optical *z*-axis at (x = 0nm, y = 0nm) for the smooth and step-wise metalenses is shown in Figure 3(c, f), respectively; furthermore, the power distribution along the transversal *x*-axis at each focal length is shown as inset in the same figures. From the power distribution along the *z*-axis, the depth of focus (DF, defined as the distance at which the power from the FL has decayed half of its peak value along the optical axis), is $8\lambda_0$ and $7.22\lambda_0$, for the smooth and step-wise metalenses, respectively. These large values of DF are expected due to the detrimental influence of the lateral waveguides, as explained before. Finally, the transversal full-width at half-maximum (FWHM, defined as the distance at which the power at the FL has decayed half of its maximum along the transversal axis) is $1.04\lambda_0$ and $0.98\lambda_0$ for each design, respectively, demonstrating that similar results can be obtained with both structures.

3.2. Zoned metalens

In the light of the previous section, keeping the length of the lens as small as possible to avoid overlapping between Fabry-Perot and ENZ regimes seems critical. Hence, in this section an ENZ zoned metalens is designed by using the metal-dielectric-metal plasmonic waveguide with the same dimensions as the previous metalenses.

The zoning technique has been used in the design of classical metallic lenses.[26] Also, this

technique has been applied to dielectric lenses where are commonly known as Fresnel lenses.[27] This concept has been commonly applied in the design of zoned dielectric lenses and it has been proposed and experimentally demonstrated at millimeter-waves in all-metallic fishnet metalenses.[28–31] The zoning technique relies on the fact that redundant phase advance of 2π of the waves traveling inside of the lens does not contribute to the focusing. Thus, the lens section causing it can be removed. This effectively results into a lens with a saw-tooth profile with a maximum tooth length (t) given by:

$$t = \frac{\lambda_0}{1-\sqrt{\varepsilon_{lens}}} \tag{2}$$

where ε_{lens} is the permittivity of the lens. We can calculate the profile of a zoned lens by using this length limit along with the general equation of a conical section following the Fermat's principle which also depends on the permittivity of the medium used for the lens. It can be written as follows:[32]

$$\left(1-\varepsilon_{lens}\right)\left(z+mt\right)^2 - 2\left(FL+mt\right)\left(1-\sqrt{\varepsilon_{lens}}\right)\left(z+mt\right) + x^2 = 0 \tag{3}$$

Were m is an integer representing the full profile (m = 0) and the successive steps of the zoned profile (m = 1,2,3,…).

By using (2) and (3) the zoned metalens is designed at the same FL and wavelength as the previous metalenses with $\varepsilon_{lens} = \varepsilon_{eff} = 0.09$ (calculated in section 2) and the resulting profile is shown in Figure 4(a). The numerical evaluation is performed with the same simulation setup as in the previous section.

The power distribution on the xz-plane at the design frequency is shown in Figure 4(b). A focus emerges at FL = $11.3\lambda_0$. This represents a small deviation of $0.56\lambda_0$ with respect to the design FL and a significant improvement compared to the smooth and step-wise metalenses from the previous section. All this improvement arises from keeping the length of each plasmonic waveguide almost identical and reduced (compared with the large differences in length shown in the previous metalenses). This ensures that the Fabry-Perot resonances appear at similar wavelengths (and relatively far from the spectrum of interest), and thus, the differences between Drude responses of each waveguide to be negligible. Finally, the power distribution along the optical z-axis and along the transversal x-axis at the resulting FL is shown in Figure. 4(c). The results for the DF and FWHM for this design are $3\lambda_0$ and $0.69\lambda_0$, respectively, which demonstrate the outperformance of this design. Also, a remarkable reduction of volume of 42.91% is obtained using this design, in comparison with the full concave

metalens, which has obvious practical implications.

3.3. Graded Index (GRIN) metalens

In the previous section, it has been shown that the performance of the lens can be improved using the zoning technique. One could postulate that a further improvement could be achieved provided all waveguides had the same length. This can be achieved under a GRIN design, whereby the dimension of h_x is engineered for each waveguide across the array. In this technique, both (input and output) faces of the metalens are planar and the required phase distribution to focus the incoming plane-wave should be introduced by each waveguide in the array.[15,16,33] As it has been explained in section 2, by correctly engineering h_x, different values of propagation constant and phase will be obtained. The phase that each waveguide should introduce for optical focusing can be calculated as follows:[15,34]

$$\Delta\varphi_{(m)} = \beta_{(m)} l_z = \beta_0 l_z - k_o\left[\sqrt{(FL)^2 + (md_x)^2} - FL\right] + 2\pi n \qquad (4)$$

where $\Delta\varphi_{(m)}$ is the phase that should be introduced by the m^{th} waveguide in the array and n is an integer number (n = 1,2,3…). The propagation constant for each waveguide is extracted from (4) and introduced in (1) in order to calculate each dielectric thickness (h_x) to produce the required phase distribution. The resulting GRIN-ENZ plasmonic plano-concave lens is then designed and it is schematically shown in Figure 5(a).

This metalens is numerically evaluated using the same simulation setup as before. The power distribution on the *xz*-plane at the design wavelength is shown in Figure 5(b). For this metalens, the FL is obtained at $10.23\lambda_0$, which is even closer to the designed FL compared with the previous metalenses with a deviation of $0.52\lambda_0$. Also, the normalized power distribution along the optical *z*-axis and along the transversal *x*-axis at the FL is shown in Figure 5(c). Regarding the resolution of the metalens, the DF and FWHM are $2.84\lambda_0$ and $0.58\lambda_0$, respectively, with an improved resolution for this design. Finally a reduction of volume of 52.3% is obtained with this design (compared with the volume of the full concave metalens) improving at the same time the spatial resolution.

4. Discussion

In this section a summary of the results for all the metalenses is presented in order to compare them quantitatively. The results of the FL, DF, FWHM and volume for each lens are shown in Table 1.

Lens profile	FL[a] (λ_0)	DF[b] (λ_0)	FWHM[c] (λ_0)	Volume(%)[d]
Smooth concave	14.4	8	1.04	100
Step-wise concave	14.23	7.22	0.98	103
Zoned	11.3	3	0.69	57.09
GRIN	10.23	2.84	0.58	47.74

[a] FL is the Focal length.
[b] DF is the Depth of focus.
[c] FWHM is the full-width at half-maximum along the transversal *x*-axis at the FL.
[d] The volume of each lens has been normalized to the volume of the smooth concave metalens.

Note that, in general terms, the best performances are obtained with the zoned and GRIN metalenses with a reduction of volume of 42.91% and 52.3%, respectively, which is an advantage in order to use these designs in integrated systems. It is important to highlight that all designs here shown are diffraction limited since they do not operate in the near-field of the metalens. An improved resolution (e.g. super resolution) of the metalenses may be, however, obtained using different techniques [35] but it is beyond of the scope of this manuscript.

5. Conclusions

In this work, metal-dielectric-metal plasmonic waveguides working near cut-off of the transverse electric TE_1 mode have been used to emulate an ENZ medium. It has been shown that the ENZ wavelength can be changed according to the dielectric thickness. This plasmonic waveguide working as an effective ENZ medium has been used in the design of several metalenses: a plano-concave smooth-profiled metalens and its step-wise approximation, a zoned metalens, and graded index (GRIN) metalens. Numerical results demonstrate that the best performances in terms of FL, DF and FWHM are obtained for the latter two cases with a reduction of volume (compared with the volume of the full concave metalens) of 42.91% and 52.3% for the zoned and GRIN designs, respectively. Experimental demonstration of these findings is expected in the near future.

ACKNOWLEDGMENTS

This work was supported by the Spanish Ministerio de Economía y Competitividad under contract TEC2014-51902-C2-2-R. V.P.-P. is sponsored by Spanish Ministerio de Educación, Cultura y Deporte under grant FPU AP-2012-3796. M. N.-C. is supported by the Birmingham Fellowship. M.B. is sponsored by the Spanish Government via RYC-2011-08221.

REFERENCES

[1] N. Engheta and R. Ziolkowski, *Metamaterials:Physics and Engineering Explorations*, 1st ed. (John Wiley & Sons & IEEE Press, USA, 2006).

[2] R. Marqués, F. Martín, and M. Sorolla, *Metamaterials with Negative Parameters: Theory, Design and Microwave Applications* (Hoboken. NJ: Wiley, 2008).

[3] A. Sihvola, S. Tretyakov, and A. Baas, J. Commun. Technol. Electron. **52**, 986 (2007).

[4] M. Silveirinha and N. Engheta, Phys. Rev. Lett. **97**, 157403 (2006).

[5] M. Silveirinha and N. Engheta, Phys. Rev. B **76**, 245109 (2007).

[6] B. Edwards, A. Alù, M.E. Young, M. Silveirinha, and N. Engheta, Phys. Rev. Lett. **100**, 1 (2008).

[7] D. Powell, A. Alù, B. Edwards, A. Vakil, Y. Kivshar, and N. Engheta, Phys. Rev. B **79**, 245135 (2009).

[8] G. Subramania, a. J. Fischer, and T.S. Luk, Appl. Phys. Lett. **101**, 241107 (2012).

[9] R. Maas, J. Parsons, N. Engheta, and A. Polman, Nat. Photonics **7**, 907 (2013).

[10] J. Gao, L. Sun, H. Deng, C.J. Mathai, S. Gangopadhyay, and X. Yang, Appl. Phys. Lett. **103**, 051111 (2013).

[11] A. Alù and N. Engheta, Phys. Rev. B **78**, 15 (2008).

[12] N. Engheta, Science **317**, 1698 (2007).

[13] M. Navarro-Cía, M. Beruete, M. Sorolla, and N. Engheta, Phys. Rev. B **86**, 165130 (2012).

[14] A. Alù, M. Silveirinha, A. Salandrino, and N. Engheta, Phys. Rev. B **75**, 155410 (2007).

[15] V. Torres, V. Pacheco-Peña, P. Rodríguez-Ulibarri, M. Navarro-Cía, M. Beruete, M. Sorolla, and N. Engheta, Opt. Express **21**, 9156 (2013).

[16] V. Pacheco-Peña, V. Torres, M. Beruete, M. Navarro-Cía, and N. Engheta, J. Opt. **16**, 094009 (2014).

[17] V. Pacheco-Peña, V. Torres, B. Orazbayev, M. Beruete, M. Navarro-Cía, M. Sorolla, and N. Engheta, Appl. Phys. Lett. **105**, 243503 (2014).

[18] V. Torres, B. Orazbayev, V. Pacheco-Peña, J. Teniente, M. Beruete, M. Navarro-Cia, M. Sorolla, and N. Engheta, IEEE Trans. Antennas Propag. (2015).

[19] W. Rotman, IRE Trans. Antennas Propag. **10**, 82 (1962).

[20] E.D. Palik, *Handbook of Optical Constants of Solids* (Academic, 1985).

[21] K.Y. Kim, Y.K. Cho, H.-S. Tae, and J.-H. Lee, Opt. Express **14**, 320 (2006).

[22] A. Alù and N. Engheta, J. Opt. Soc. Am. B **23**, 571 (2006).

[23] C. Argyropoulos, P.Y. Chen, G. D'Aguanno, N. Engheta, and A. Alù, Phys. Rev. B - Condens. Matter Mater. Phys. **85**, 045129 (2012).

[24] R. Fleury and A. Alù, Phys. Rev. B **87**, 201101 (2013).

[25] D.R. Smith, D.C. Vier, T. Koschny, and C.M. Soukoulis, Phys. Rev. E **71**, 036617 (2005).

[26] W.E. Kock, Proc. IRE **34**, 828 (1946).

[27] H.D. Hristov, *Fresnel Zones in Wireless Links, Zone Plate Lenses and Antennas* (Artech House, Inc., Norwood, MA, 2000).

[28] V. Pacheco-Peña, B. Orazbayev, V. Torres, M. Beruete, and M. Navarro-Cía, Appl. Phys. Lett. **103**, 183507 (2013).

[29] V. Pacheco-Peña, B. Orazbayev, U. Beaskoetxea, M. Beruete, and M. Navarro-Cía, J. Appl. Phys. **115**, 124902 (2014).

[30] B. Orazbayev, V. Pacheco-Peña, M. Beruete, and M. Navarro-Cía, Opt. Express **23**, 8555 (2015).

[31] V. Pacheco-Peña, M. Navarro-Cía, B. Orazbayev, I. V Minin, O. V Minin, and M. Beruete, IEEE Trans. Antennas Propag. **63**, 3710 (2015).

[32] M. Navarro-Cía, M. Beruete, I. Campillo, and M. Sorolla, IEEE Trans. Antennas Propag. **59**, 2141 (2011).

[33] R.B. Greegor, C.G. Parazzoli, J.A. Nielsen, M.A. Thompson, M.H. Tanielian, and D.R. Smith, Appl. Phys. Lett. **87**, 091114 (2005).

[34] P.F. Goldsmith, *Quasioptical Systems: Gaussian Beam Quasioptical Propagation and Applications* (Wiley-IEEE Press, 1997).

[35] E.T.F. Rogers, J. Lindberg, T. Roy, S. Savo, J.E. Chad, M.R. Dennis, and N.I. Zheludev, Nat. Mater. **11**, 432 (2012).

VITAE

Víctor Pacheco-Peña

Was born in San Salvador, El Salvador, in 1988. He received the degree in Telecommunication engineering from Universidad Don Bosco (UDB), Soyapango, El Salvador, in 2011.

He received the M.Sc. degree in communication technologies from the Public University of Navarre, Navarre, Spain, in 2012. He is currently working as a Predoctoral Researcher (FPU fellowship recipient) with the Antennas Group-TERALAB in the Electrical and Electronic Engineering Department, Public University of Navarre, Pamplona, Spain. His current research interests are mainly aimed on metamaterials, permittivity near zero structures, extraordinary transmission applications, lenses and millimeter and terahertz frequencies.

Miguel Navarro-Cía

Was born in Pamplona, Spain, in 1982. He received the M.Sci. and Ph.D. degrees in Telecommunication Engineering, and M.Res. degree in Introduction to Research in Communications from Universidad Pública de Navarra, Spain, in 2006, 2010 and 2007, respectively.

From September 2006 to January 2010, and from February 2010 until March 2011, he worked as a Predoctoral Researcher (FPI fellowship recipient) and a Research & Teaching Assistant in the Electrical and Electronic Engineering Department, Universidad Pública de Navarra, respectively. He was a Research Associate at Imperial College London and University College London in 2011 and 2012, respectively, and a Junior Research Fellow at Imperial College London from December 2012 until November 2015. Currently he is Birmingham Fellow in the School of Physics and Astronomy, University of Birmingham. He is also affiliated as a Visiting Researcher with Imperial College London and University College London. He worked as a Visiting Researcher at University of Pennsylvania for 3 months in 2010, at Imperial College London (In the departments of Physics and Materials) in 2008, 2009 and 2010 for 4, 6 and 3 months, respectively, and at Valencia Nanophotonics Technology Center for 2 months in 2008. His current research interests are focused on plasmonics, near-field time-domain spectroscopy, metamaterials, antennas, complex surface waves, frequency selective surfaces, and millimeter, terahertz and infrared frequencies. Dr. Navarro-Cía is senior member of the IEEE and member of the Optical Society of America, the European Association on Antennas and Propagation (EurAAP), and the Spanish National Association and Professional Board of Telecommunication Engineers. He was awarded with the Best Doctoral Thesis in Basic Principles and Technologies of Information and Communications, and Applications corresponding to the XXXI Edition of Awards "Telecommunication Engineers" 2010 and the 2012 CST University Publication Awards to the best international journal publication using CST Microwave Studio™ and was recipient of the 2011 Junior Research Raj Mittra Travel Grant.

Miguel Beruete

Was born in Pamplona, Spain, in 1978. He received the M.Sci. and Ph.D. degrees in telecommunication engineering, from the Public University of Navarre (UPNA), Navarre, Spain, in 2002 and 2006, respectively.

From September 2002 to January 2007, he was working as Predoctoral Researcher (FPI

fellowship recipient) in the Electrical and Electronic Engineering Department, Public University of Navarre. From January to March 2005 he worked as visiting researcher at the University of Seville, as a part of his doctoral research.

From February 2007 to September 2009 he was at the electronics department of the technological center CEMITEC in Noain (Navarre), developing, designing and measuring high frequency communication devices.

In September 2009 he joined the TERALAB at UPNA, as a post-doc Ramón y Cajal fellow researcher under the supervision of Prof. Mario Sorolla.

In March 2014, he joined the Antennas Group-TERALAB of UPNA, where he supervises several Ph.D. and M.Sci. Theses and heads the TERALAB laboratory.

Dr. Beruete has authored near 100 JCR articles, 2 book chapters, 3 patents and near 250 conference communications. He has been awarded with the PhD Prize of the Public University of Navarre (2006-2007) to the best Doctoral Thesis in the year 2006-2007, 2 CST University Publication Awards to the best international journal publication using CST in the years 2005 and 2012, and the XII Talgo Award of Technological Innovation in 2011. His research interests include metamaterials, plasmonics, extraordinary transmission structures, leaky-wave antennas, nanoantennas, and in general quasioptical devices from microwaves to infrared frequencies, with special interest in the terahertz range.

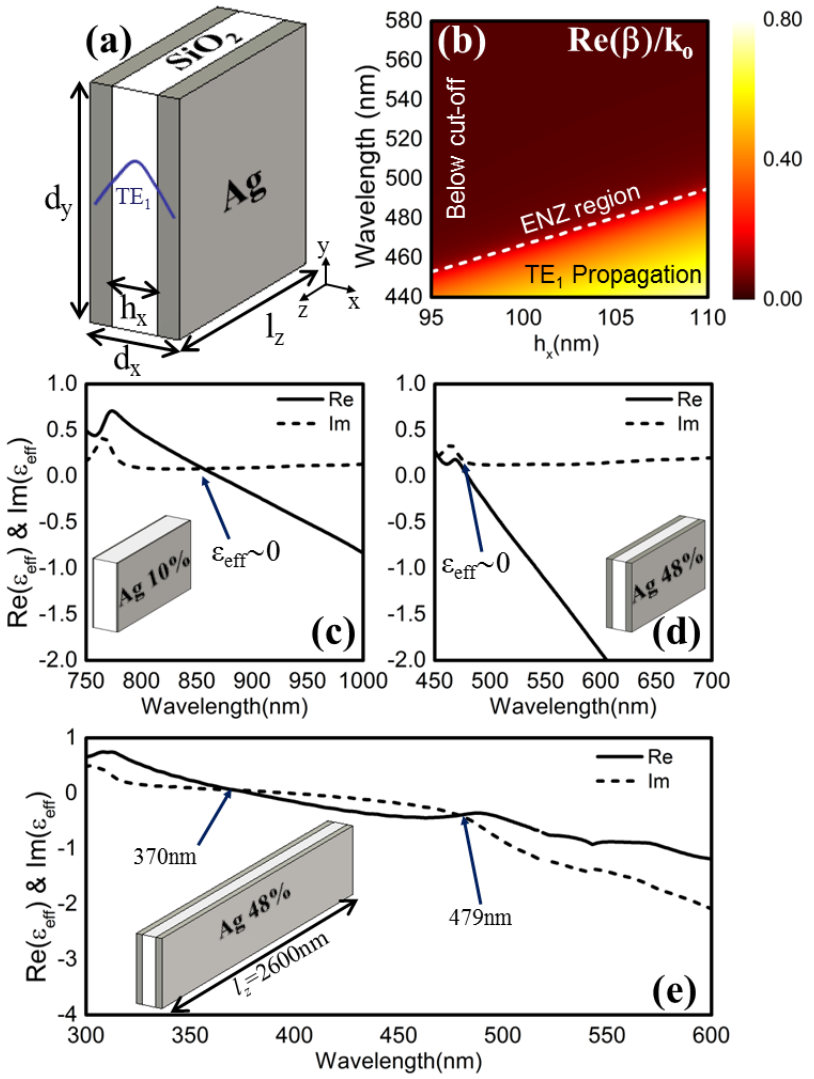

FIG. 1. (a) Schematic representation of the metal-dielectric-metal plasmonic waveguide with thickness d_x = 200 nm, length l_z = 1000 nm, height d_y = 500 nm and dielectric thickness h_x. (b) Analytical results of the normalized real part of β of the transverse electric TE_1 mode with respect to k_0 as a function of the operational wavelength and thickness of the dielectric. Retrieved values of the complex effective permittivity for the case of a waveguide with metal thickness of 10% (c), 48%(d) and 48% with a length of l_z = 2600 nm (e).

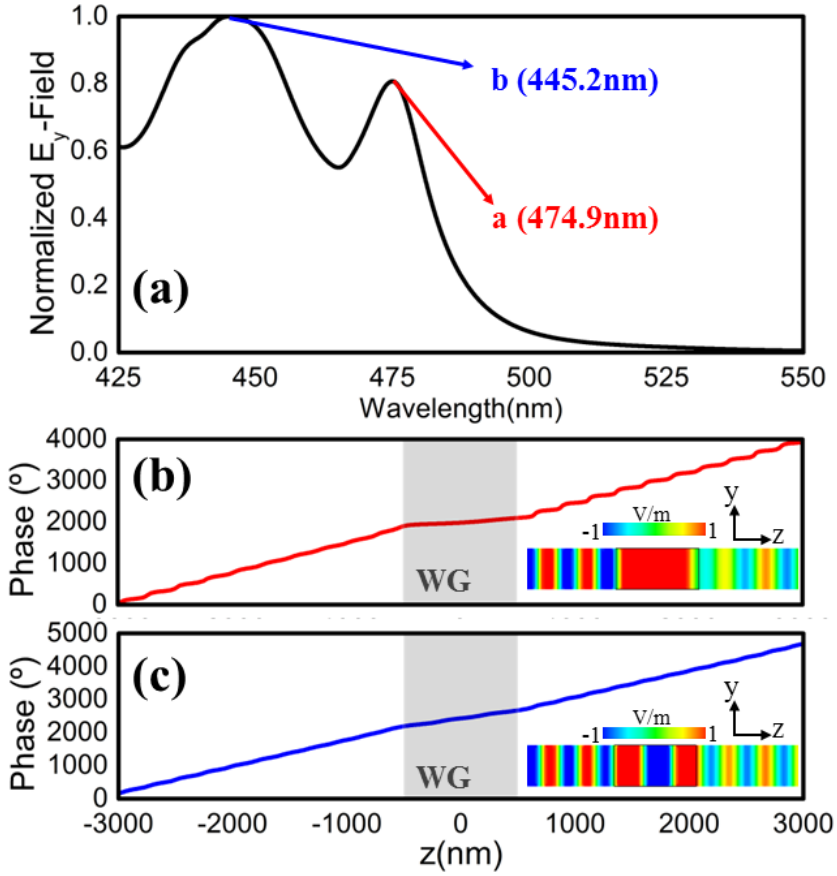

FIG. 2. (a) Numerical results of the normalized E_y-field at the output of the parallel plate plasmonic waveguide with a dielectric thickness of h_x = 104nm corresponding to a 48% of metal. Numerical results of the phase distribution of the E_y-field along the optical axis z for the first two peaks of transmission of the top panel: (b) at 474.9nm and (c) at 445.2 nm, along with the normalized field distribution on the yz-plane for each case (bottom-right inset).

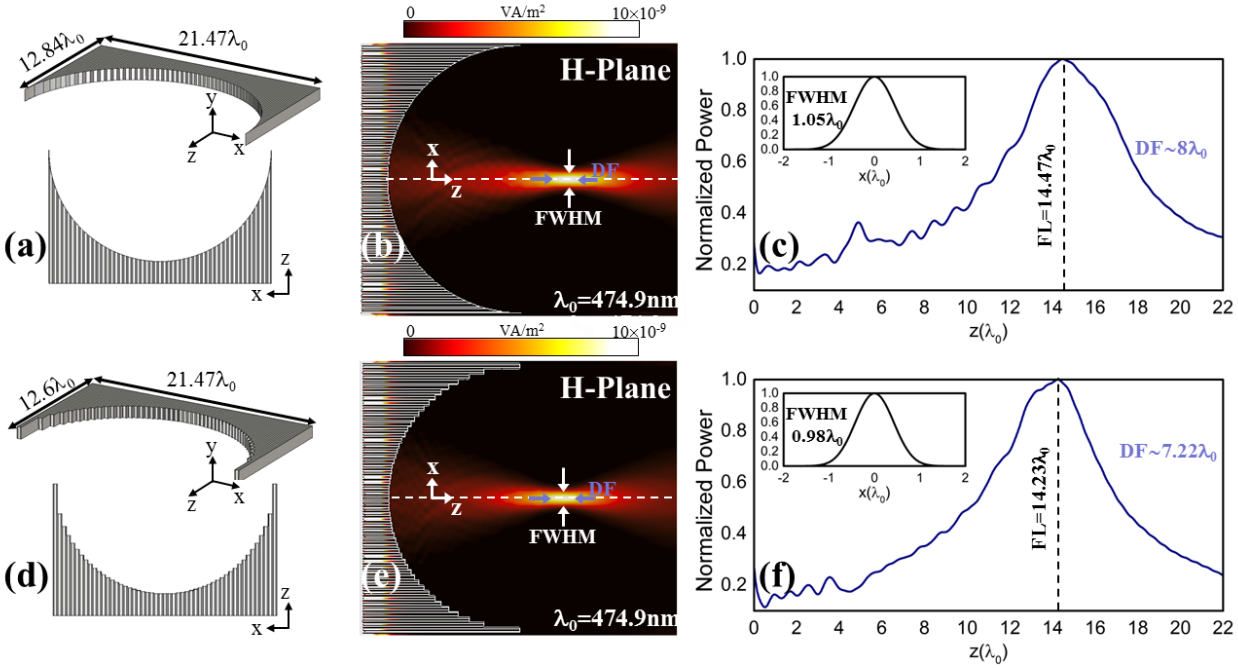

FIG. 3. Schematic representation of the plano-concave smooth profiled metalens (a) and the step-wise metalens (d). Numerical results of the power distribution on the *xz*-plane at the designed wavelength λ_0 = 474.9 nm for the smooth profiled metalens (b) and step-wise metalens (e). Numerical results of the normalized power distribution along the optical *z*-axis for the smooth profiled metalens (c) and step-wise metalens (f) together with the normalized power distribution along the transversal *x*-axis at each focal length (shown as inset).

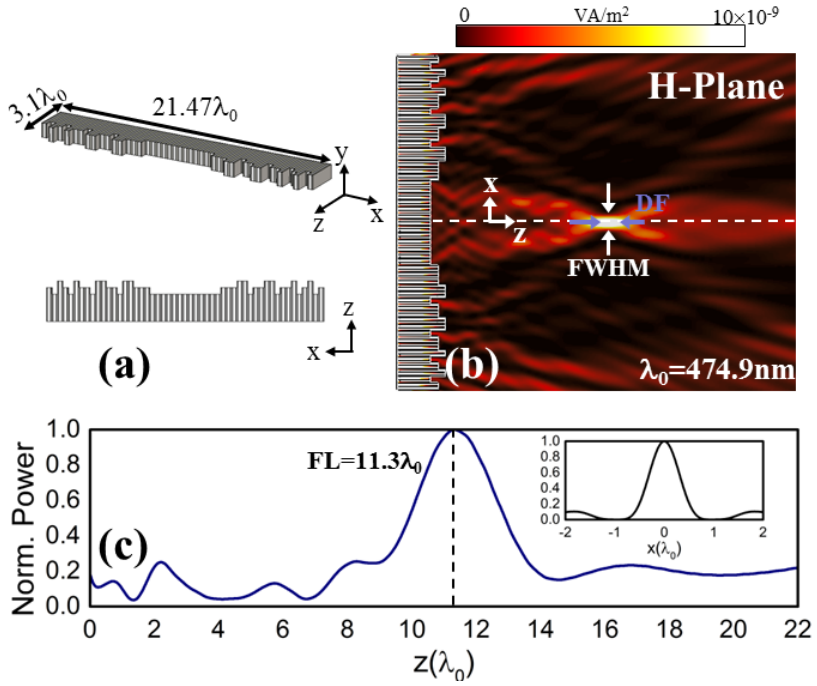

FIG. 4. (a) Schematic representation of the zoned metalens. (b) Numerical results of the power distribution on the *xz*-plane at the designed wavelength λ_0 = 474.9 nm for zoned metalens. (c) Numerical results of the normalized power distribution along the optical *z*-axis for the zoned metalens along with the normalized power distribution along the transversal *x*-axis at the focal length (shown as inset).

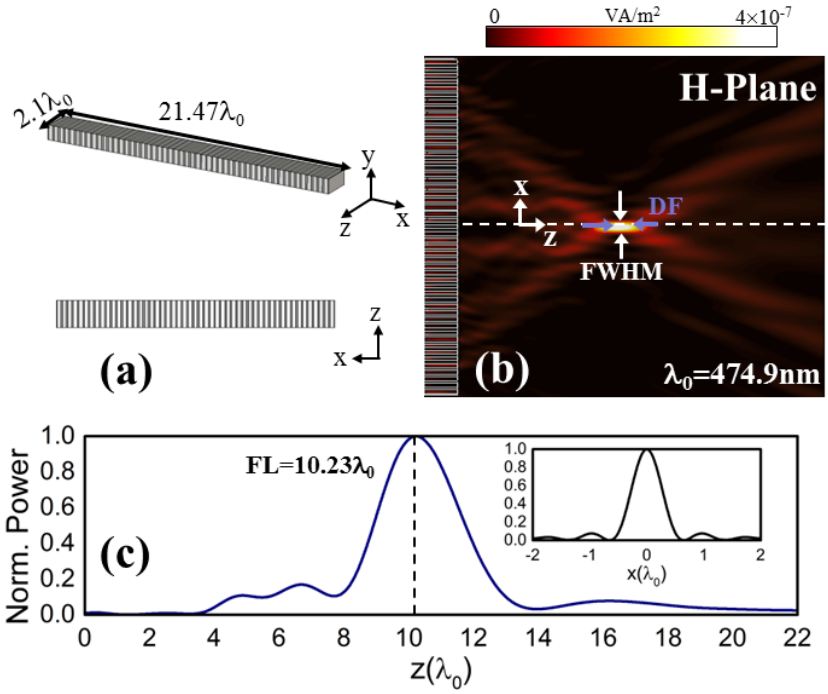

FIG. 4. (a) Schematic representation of designed GRIN metalens. (b) Numerical results of the power distribution on the *xz*-plane at the designed wavelength λ_0 = 474.9 nm for GRIN metalens. (c) Numerical results of the normalized power distribution along the optical *z*-axis for the GRIN metalens along with the normalized power distribution along the transversal *x*-axis at the focal length (shown as inset).